Cell Reports

Article

Divergent Nodes of Non-autonomous UPR^{ER} Signaling through Serotonergic and Dopaminergic Neurons

Graphical Abstract

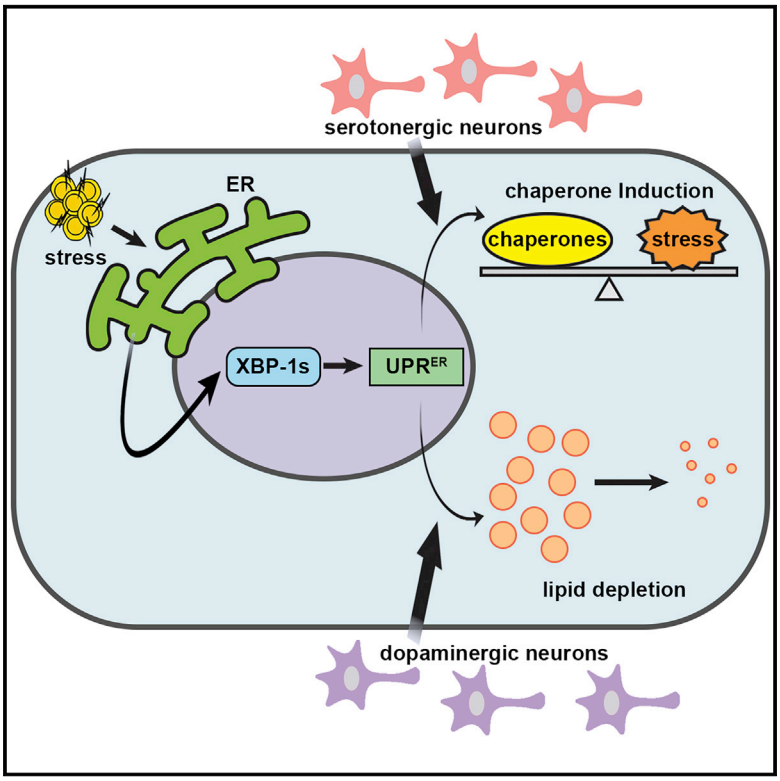

Highlights

- Non-autonomous signaling of UPR^{ER} is mediated by serotonergic and dopaminergic neurons
- Serotonergic neurons drive protein homeostasis to extend lifespan
- Dopaminergic neurons drive lipid homeostasis to extend lifespan

Authors

Ryo Higuchi-Sanabria, Jenni Durieux, Naame Kelet, ..., Sarah U. Tronnes, Larry Joe, Andrew Dillin

Correspondence

dillin@berkeley.edu

In Brief

Higuchi-Sanabria et al. identify two distinct neuronal populations that are critical in signaling non-autonomous UPR^{ER} from neurons to the periphery: serotonergic neurons drive induction of protein changes and dopaminergic neurons drive induction of lipid changes.

Higuchi-Sanabria et al., 2020, Cell Reports *33*, 108489
December 8, 2020
https://doi.org/10.1016/j.celrep.2020.108489

CellPress

Cell Reports

CellPress
OPEN ACCESS

Article

Divergent Nodes of Non-autonomous UPR^{ER} Signaling through Serotonergic and Dopaminergic Neurons

Ryo Higuchi-Sanabria,[1,4] Jenni Durieux,[1,4] Naame Kelet,[1] Stefan Homentcovschi,[1] Mattias de los Rios Rogers,[1] Samira Monshietehadi,[1] Gilberto Garcia,[1] Sofia Dallarda,[1] Joseph R. Daniele,[2] Vidhya Ramachandran,[1] Arushi Sahay,[1] Sarah U. Tronnes,[3] Larry Joe,[1] and Andrew Dillin[1,5,*]

[1]Department of Molecular & Cellular Biology, Howard Hughes Medical Institute, The University of California, Berkeley, Berkeley, CA 94720, USA

[2]TRACTION, The University of Texas MD Anderson Cancer Center, South Campus Research, Houston, TX 77054, USA

[3]Department of Molecular, Cellular, and Developmental Biology, University of Colorado, Boulder, Boulder, CO 80309, USA

[4]These authors contributed equally

[5]Lead Contact

*Correspondence: dillin@berkeley.edu

https://doi.org/10.1016/j.celrep.2020.108489

SUMMARY

In multicellular organisms, neurons integrate a diverse array of external cues to affect downstream changes in organismal health. Specifically, activation of the endoplasmic reticulum (ER) unfolded protein response (UPR^{ER}) in neurons increases lifespan by preventing age-onset loss of ER proteostasis and driving lipid depletion in a cell non-autonomous manner. The mechanism of this communication is dependent on the release of small clear vesicles from neurons. We find dopaminergic neurons are necessary and sufficient for activation of cell non-autonomous UPR^{ER} to drive lipid depletion in peripheral tissues, whereas serotonergic neurons are sufficient to drive protein homeostasis in peripheral tissues. These signaling modalities are unique and independent and together coordinate the beneficial effects of neuronal cell non-autonomous ER stress signaling upon health and longevity.

INTRODUCTION

Under conditions of stress, multicellular organisms must coordinate an effective response across diverse tissues to maintain organismal homeostasis. For most stress responses, including the endoplasmic reticulum (ER) unfolded protein response (UPR^{ER}), there is an age-associated decline in protein folding and the proteotoxic stress response. This can be circumvented by overexpressing the primary transcription factor *xbp-1s*, which can preserve organismal health and extend lifespan (Frakes and Dillin, 2017; Higuchi-Sanabria et al., 2016; Taylor and Dillin, 2013). In particular, overexpression of spliced *xbp-1* (*xbp-1s*) specifically in the *Caenorhabditis elegans* nervous system extended lifespan and increased ER stress tolerance in a cell non-autonomous manner by promoting protein homeostasis (Frakes et al., 2020; Taylor and Dillin, 2013) and driving lipid homeostasis (Daniele et al., 2020; Imanikia et al., 2019a). Although the identity of the secreted ER-stress signal (SERSS) from neurons to the periphery required in this paradigm is still unknown, small clear vesicles (SCVs), which could be host to numerous neurotransmitters and biogenic amines, were implicated in neurons, whereas dense core vesicles (DCVs), which are host to numerous neuropeptides, were implicated in glia (Frakes et al., 2020; Taylor and Dillin, 2013).

Downstream of the SERSS, the intestine activates UPR^{ER} in an *xbp-1s*-dependent manner, which contributed to the lifespan extension found in this paradigm. Previously, the beneficial effect of neuronal non-autonomous UPR^{ER} induction in the periphery was ascribed to increased protein homeostasis by upregulation of chaperones (Taylor and Dillin, 2013). However, by characterizing the specific changes that occur in the signal receiving cell, namely, the intestine, it was uncovered that this neuronal signal results in significant ER expansion and lipid depletion. These phenomena are chaperone independent and are both necessary and sufficient for the lifespan extension found when *xbp-1 s* is overexpressed in neurons (Daniele et al., 2020). Thus, neuronal *xbp-1 s* activates two distinct pathways in the distal tissue: a protein homeostasis arm through chaperone induction and a metabolic arm that involves ER remodeling and lipid depletion. The depletion of lipids occurs by two mechanisms: (1) upregulation of lysosomal lipases and desaturases, which depletes triglycerides and increases oleic acid levels (Imanikia et al., 2019a); and (2) activation of lipophagy by a conserved RME-1/RAB-10/EHBP-1 complex (Daniele et al., 2020). However, how these two distinct signals are elicited and the neural subtypes involved in these divergent mechanisms are yet to be discovered.

A similar communication from neurons to periphery is also observed in vertebrates. When *Xbp1s* is overexpressed in *Pomc* neurons of the hypothalamus of mice, the UPR^{ER} is upregulated and has beneficial impacts on metabolic physiology (e.g., improved glucose levels, improved insulin sensitivity, and

protection against high-fat diet-induced obesity) (Williams et al., 2014). In this model, *Xbp1s* increases *Pomc* neuron activity, which in turn increases energy expenditure by promoting brown adipose tissue (BAT) thermogenesis and browning of white adipose tissue (WAT), which results in an overall decrease in fat mass and body weight, consistent with the findings in *C. elegans*. The direct conservation of these phenomena downstream of neuronal *Xbp1s* suggests that mechanistic understanding of the neuronal circuits and cellular changes in response to these signals would serve as a critical foundation for understanding age- and disease-linked declines in ER homeostasis and ER quality control.

Here, we performed screens to identify the specific neurons important for sensing and transmitting UPR^{ER} to the periphery. These studies specifically segregate two distinct and independent mechanisms of UPR^{ER} through two separate sets of neurons: protein homeostasis through chaperone induction by serotonin signaling and metabolic remodeling through lipid depletion by dopamine signaling. These phenomena are generally discussed as simultaneous and interchangeable responses to UPR^{ER} activation. However, we challenge this notion to argue not only that they can be separated but also that unique machinery exist to elicit these divergent responses.

RESULTS

Screening of Neurotransmitters Reveal Serotonin Signaling as Necessary and Sufficient for Chaperone Induction of Non-autonomous UPR^{ER}

The goal of this study was to identify specific neuronal subtypes involved in the cell non-autonomous transmission of UPR^{ER}. Our lab described a requirement for neurotransmitter release by SCVs to promote cell non-autonomous signaling downstream of *xbp-1 s* (Salio et al., 2006; Taylor and Dillin, 2013). Thus, using high intestinal expression of the putative UPR^{ER} reporter *hsp-4p::GFP* as the readout of cell non-autonomous UPR^{ER} induction, we crossed these reporter animals to a panel of mutants for neurotransmitter biosynthesis and function to screen for mutations that prevent non-autonomous UPR^{ER} signaling. Specifically, pan-neuronal overexpression of the active, spliced variant of *xbp-1*, *xbp-1s* (referred to as neuronal *xbp-1s* animals), resulted in robust activation of UPR^{ER} and induction of the *hsp-4p::GFP* reporter. Suppressors of non-autonomous UPR^{ER} induction can be visualized as a loss of fluorescence using this reporter. Screening a panel of neurotransmitter mutants identified mutations in *mec-3*, *tph-1*, and *unc-30* as strong suppressors of non-autonomous UPR^{ER} induction (Figure 1A).

The *mec-3* gene encodes a LIM homeobox protein, and mutations in *mec-3* specifically affect sensory neurons and decrease glutamatergic signaling (Serrano-Saiz et al., 2013; Xue et al., 1992). *tph-1* encodes the tryptophan hydroxylase enzyme, which is a key enzyme for serotonin biosynthesis; animals with *tph-1* mutations fail to synthesize serotonin (Sze et al., 2000). *unc-30* plays a critical role in GABA synthesis, and mutations in *unc-30* have severe defects in GABAergic differentiation, axon guidance, and downstream motor/behavioral phenotypes (Westmoreland et al., 2001). Among these three neuronal circuits, only serotonin signaling has been described to be critical in promoting neurotransmission of stress signals, including the UPR of the mitochondria (UPR^{MT}) (Berendzen et al., 2016) and the heat-shock response (HSR) (Tatum et al., 2015). Furthermore, the loss of *tph-1* did not cause gross morphological changes to the organism, such as *mec-3* and *unc-30* mutations, which cause severe motor defects. Moreover, further quantitative analysis of reporters normalized to animal size revealed significant differences ($p < 0.001$) for only *tph-1* and *unc-30* mutations (Figure 1B). Therefore, we sought to further characterize serotonin signaling as a potential "master regulator" of stress signaling and thus playing a similar role in mediating neurotransmission of the UPR^{ER} to the periphery. First, we confirmed that the deletion mutant *tph-1(mg280)* failed to promote non-autonomous UPR^{ER} signaling, as measured by *hsp-4p::GFP* induction across a large population by quantification using a large-particle biosorter (Figure 1C; Daniele et al., 2017). More importantly, mutations in *tph-1* fully suppressed the lifespan extension found in neuronal *xbp-1s* animals, providing strong evidence that serotonin signaling is critical for the beneficial effects of neuronal *xbp-1s* (Figure 1D).

To determine whether serotonergic neurons were sufficient to drive non-autonomous UPR^{ER} in peripheral tissue, we created transgenic animals overexpressing *xbp-1s* specifically in serotonergic neurons (*tph-1p::xbp-1s*, named serotonergic *xbp-1s*). Three independent overexpression lines of serotonergic *xbp-1s* overexpression showed robust induction of the UPR^{ER} in the periphery (Figures 2A and 2B). Moreover, the peripheral activation of the UPR^{ER} was fully dependent on serotonin production (*tph-1*), suggesting that serotonergic *xbp-1s* drives non-autonomous UPR^{ER} induction through a similar serotonin-dependent mechanism as pan-neuronal *xbp-1s* and not through some non-specific, off-target effect of serotonergic *xbp-1s* expression (Figures 2C and 2D). To determine whether the induction of chaperones in the periphery was beneficial for whole-animal physiology, we performed survival assays upon exposure to the chemical agent tunicamycin, which blocks N-linked glycosylation in the ER to produce protein misfolding stress (Heifetz et al., 1979). Indeed, we found that serotonergic *xbp-1s* animals have a significant increase in survival under ER stress, which is also fully dependent on serotonin signaling (Figures 2E and 2F). Under basal conditions, serotoninergic *xbp-1s* animals also exhibited a mild lifespan extension, which is also dependent on serotonin signaling (Figures S1A and S1B). Both the lifespan extension and induction of the UPR^{ER} are dependent on *xbp-1*, as RNAi knockdown of *xbp-1* fully suppressed these phenotypes (Figures S1C–S1F). These data suggest that serotonergic *xbp-1s* is sufficient to drive non-autonomous UPR^{ER} induction in the periphery, which has direct implications in organismal physiology and lifespan.

Pan-neuronal *xbp-1s* can drive two independent arms of the UPR^{ER} in the periphery: a protein homeostasis arm by upregulation of chaperones and a metabolic arm that promotes lipid depletion through the conserved EHBP-1/RME-1/RAB-10 lipophagy machinery (Daniele et al., 2020). To determine whether serotonergic *xbp-1s* was also sufficient to drive the lipid homeostasis arm of non-autonomous UPR^{ER} induction, we used the lipid droplet marker *dhs-3p::DHS-3::GFP* to measure lipid levels in the intestine (Na et al., 2015; Zhang et al., 2012). We have previously validated that this reporter is a reliable marker that

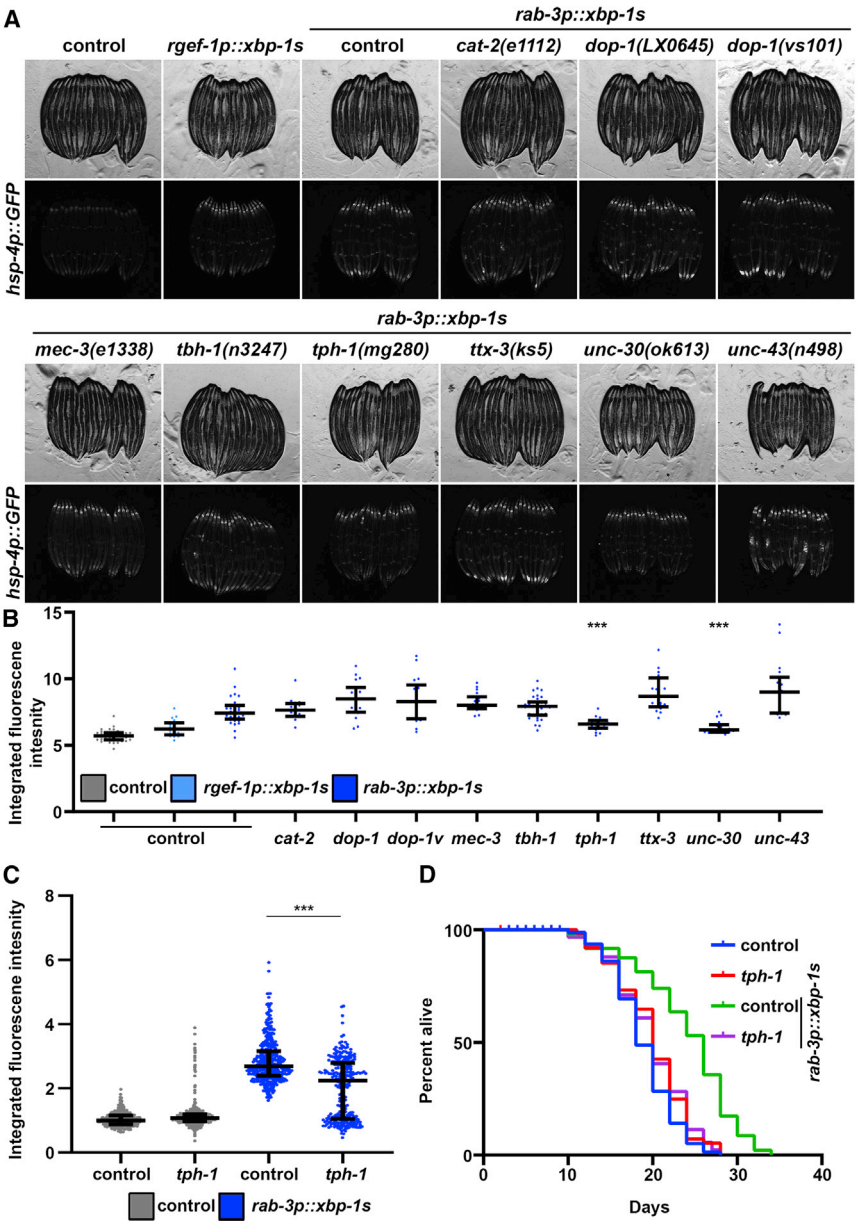

Figure 1. A Screen for Neurotransmitters Reveals Serotonin as an Essential Signal for Non-autonomous UPR^{ER} of Chaperones

(A) Fluorescent micrographs of day 1 adult *hsp-4p::GFP* control or neuronal *xbp-1s* (*rgef-1p::GFP or rab-3p::GFP*) animals carrying mutations for genes encoding neurotransmitter synthesis or signaling pathways. All images are contrast matched.

(B) Quantification of (A) using ImageJ as described in STAR Methods with control represented in gray and neuronal *xbp-1s* represented in blue (light blue, *rgef-1p::xbp-1s*; dark blue, *rab-3p::xbp-1s*). Lines represent median and interquartile range, with each dot representing a single animal. ***p < 0.001 compared to *rab-3p::xbp-1s* controls using Student's t test. *dop-1*, *dop-1(LX0645)*; *dop-1v*, *dop-1(vs101)*.

(C) Quantification of *hsp-4p::GFP* in day 1 adult *hsp-4p::GFP* control (gray) or neuronal *xbp-1s* (*rab-3p::xbp-1s*; blue) animals with and without *tph-1(mg280)* mutation for serotonin synthesis. Lines represent median and interquartile range, with each dot representing a single animal. Data are representative of three independent trials. ***p < 0.001 using non-parametric Mann-Whitney testing.

(D) Lifespans of control and neuronal *xbp-1s* (*rab-3p::xbp-1s*) animals with and without *tph-1(mg280)* mutation for serotonin synthesis. Data are representative of three independent trials. See Table S1–S2 for lifespan statistics.

correlates well with lipid levels in worms (Daniele et al., 2020). Interestingly, we found that serotonergic *xbp-1s* animals exhibit increased lipid levels and thus failed to deplete lipids (Figures S2A and S2). Moreover, unlike pan-neuronal *xbp-1s*, the lifespan extension of serotonergic *xbp-1s* is not dependent on *ehbp-1*, the gene encoding the primary lipophagy component required for lipid depletion (Figure S2C; Daniele et al., 2020). Thus, it is possible that serotonergic *xbp-1s* animals promote only the protein homeostasis arm of UPR^{ER} by chaperones and that a different set of neurons is responsible for promoting the lipid homeostasis arm of UPR^{ER}.

Finally, we sought to determine whether increased serotonin signaling itself was sufficient to drive non-autonomous UPR^{ER} induction. We used a well-validated mutant of the serotonin reuptake receptor MOD-5. Mutants of *mod-5* have been shown to exhibit increased serotonin signaling (Ranganathan et al., 2001). To our surprise, *mod-5(n3314)* mutant animals failed to induce the *hsp-4p::GFP* expression (Figures S2D and S2E). Moreover, unlike serotonergic *xbp-1s* animals, *mod-5(n3314)* animals have a very mild, non-significant increase in lipid levels (Figure S2F), suggesting that simply increasing serotonin signaling is not sufficient to phenocopy serotonergic *xbp-1s*. These data suggest that serotonin signaling is necessary, but not sufficient, for transmission of neuronal UPR^{ER} to the periphery, and it is possible that other neurotransmitters are involved in the transmission of signals from serotonergic *xbp-1s*.

Screening of Neurotransmitters Reveal Dopamine Signaling as Necessary and Sufficient for Lipid Depletion Downstream of Non-autonomous UPR^{ER}

Because serotonergic *xbp-1s* animals failed to elicit changes to lipid levels, we performed a similar screen of neurotransmitter mutants measuring whole-animal lipid levels using oil red O (Escorcia et al., 2018) in an effort to identify the neurotransmitter involved in lipid-mediated changes downstream of neuronal UPR^{ER}. As previously described (Imanikia et al., 2019a), oil red

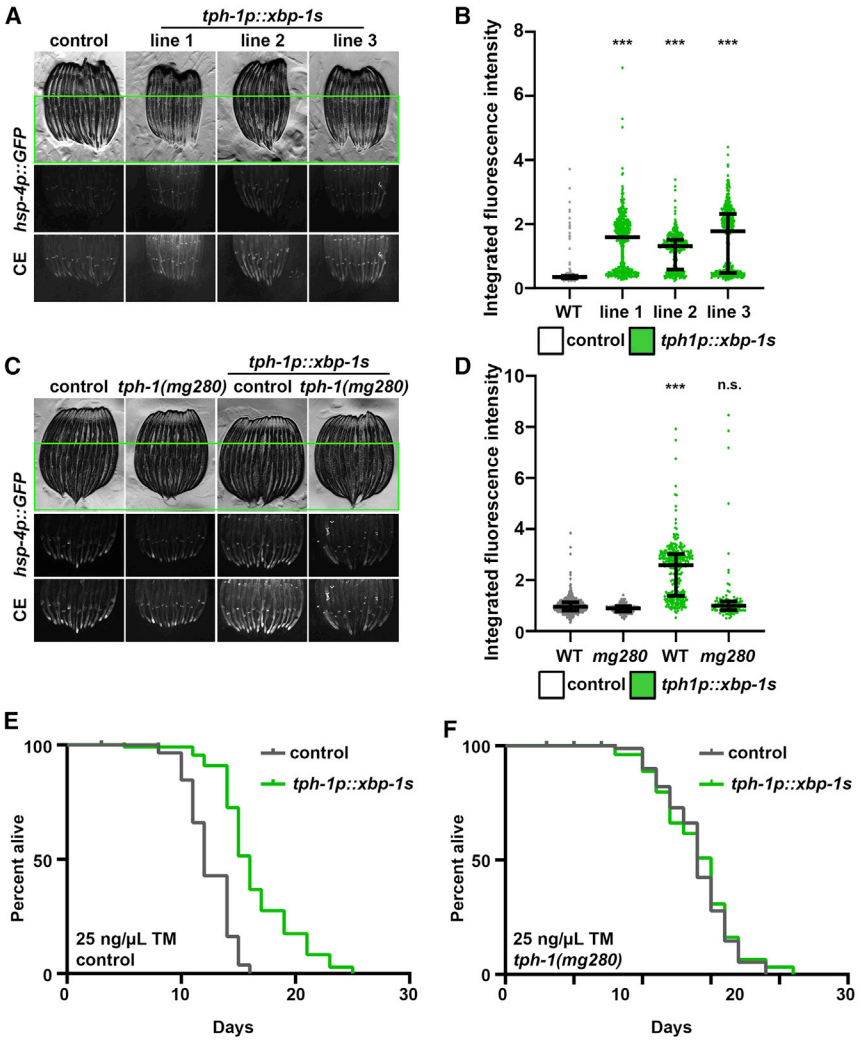

Figure 2. Serotonergic *xbp-1s* Is Sufficient to Drive Chaperone Induction and ER Stress Resistance

(A) Fluorescent micrographs of day 1 adult *hsp-4p::GFP* control or three independent integration lines of serotonergic *xbp-1s* (*tph-1p::xbp-1s*) animals. All images are contrast matched. CE, contract enhanced images for clarity; some pixels may be saturated. Only the lower 60% of the worm is shown to remove co-injection marker signal.

(B) Quantification of (A): day 1 adult *hsp-4p::GFP* control (gray) or serotonergic *xbp-1s* (*tph-1p::xbp-1s*; green) animals. Lines represent median and interquartile range, with each dot representing a single animal. Data are representative of three independent trials. ***p < 0.001 using non-parametric Mann-Whitney testing against control. Quantification is applied in the lower 60% of the worm to remove co-injection marker signal.

(C) Fluorescent micrographs of day 1 adult *hsp-4p::GFP* control or serotonergic *xbp-1s* (*tph-1p::xbp-1s*; line 3 was selected for all further analyses) animals with and without *tph-1(mg280)* mutation for serotonin synthesis. Some pixels may be saturated. Only the lower 60% of the worm is shown to remove co-injection marker signal.

(D) Quantification of (C): day 1 adult *hsp-4p::GFP* control (gray) or serotonergic *xbp-1s* (*tph-1p::xbp-1s*; green) animals. Lines represent median and interquartile range, with each dot representing a single animal. Data are representative of three independent trials. ***p < 0.001 using non-parametric Mann-Whitney testing against matching control. Quantification is applied in the lower 60% of the worm to remove co-injection marker signal.

(E) Tunicamycin (TM) survival assay of control and serotonergic *xbp-1s* (*tph-1p::xbp-1s*) animals. Animals were moved to 25 ng/µL TM plates at day 1 of adulthood. Data are representative of three independent trials. See Table S1–S2 for lifespan statistics.

(F) TM survival assay of control and serotonergic *xbp-1s* (*tph-1p::xbp-1s*) animals carrying *tph-1(mg280)* mutation for serotonin synthesis. Animals were moved to 25 ng/µL TM plates at day 1 of adulthood. Assays for (E) and (F) were performed simultaneously and can be directly compared. Data are representative of three independent trials. See Table S1–S2 for lifespan statistics.

O staining can robustly measure the decrease in lipids found in neuronal *xbp-1s* animals. Interestingly, most of the mutants tested—with the exception of serotoninergic (*tph-1*) and thermosensory (*ttx-3*) mutants—showed suppression of the decreased lipid phenotype in neuronal *xbp-1s* animals (Figures 3A and 3B). Four separate dopamine mutants exhibited suppression, two each for *cat-2* [*cat-2(n4547)* and *cat-2(e1112)*] and *dop-1* [*dop-1(vs101)* and *dop-1(LX0645)*. *cat-2* encodes for tyrosine hydroxylase, the enzyme responsible for the initial and rate-limiting step in catecholamine synthesis, including dopamine (Lints and Emmons, 1999; Nagatsu et al., 1964). *dop-1* encodes one of the dopamine receptors, which is most similar to mammalian D1-like receptor (Chase et al., 2004). Two distinct mutations in *cat-2* and *dop-1* suppressed the lipid depletion found in neuronal *xbp-1 s* animals. Moreover, several studies have already implicated dopamine signaling in fat metabolism, and increased dopamine signaling in *C. elegans* has been shown to decrease fat content through increased β-oxidation (Barros et al., 2014). Animals mutated for *dat-1*, which encodes the dopamine reuptake receptor, have increased exogenous dopamine levels, and we found that these animals also exhibited a significant decrease in lipids using the DHS-3::GFP marker (Figures S3A and S3B). Therefore, we focused our studies on lipid metabolism on dopaminergic neurons.

To directly test the requirement of dopaminergic neurons in non-autonomous UPR^{ER}, we tested the effects of overexpressed *xbp-1s* specifically in dopaminergic neurons (*dat-1p::xbp-1s*, referred to as dopaminergic *xbp-1s*). Intriguingly, these animals exhibited a significant depletion of lipids, which is dependent on dopamine synthesis (Figures 4A and 4B). However, in stark contrast to the pan-neuronal and serotonergic *xbp-1s* animals, *dat-1p::xbp-1s* animals completely failed to induce chaperones, as measured by *hsp-4p::GFP* and qPCR of *xbp-1s* downstream targets (Figures S3C–S3E). Moreover, dopaminergic *xbp-1s* was sufficient to extend lifespan in a dopamine- and *ehbp-1*-dependent manner (Figures 4C–4E). Finally, similar to serotonergic and

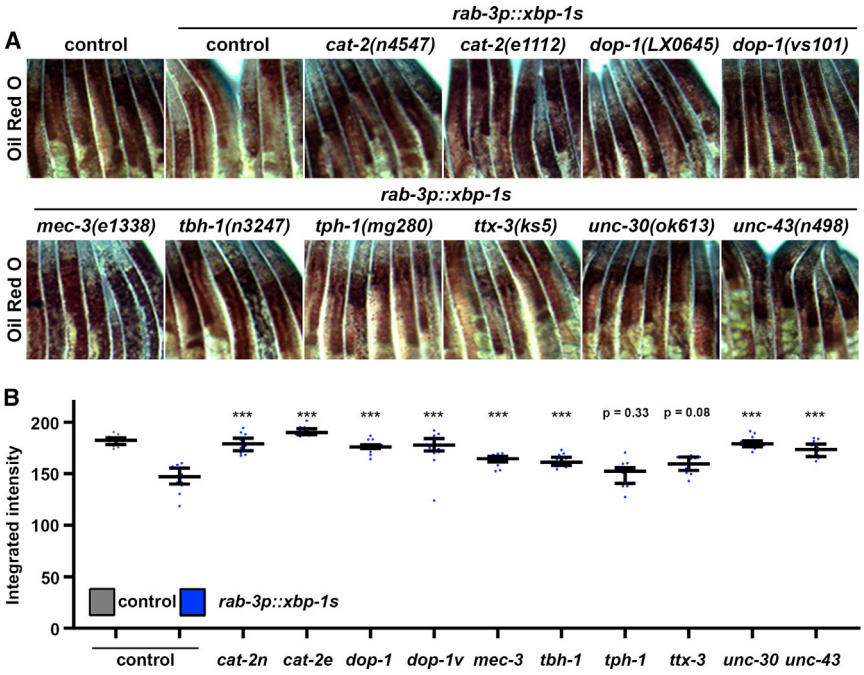

Figure 3. A Screen for Neurotransmitters Reveals Dopamine as an Essential Signal for Non-autonomous UPR^{ER} of Lipid Metabolism

(A) Brightfield micrographs of day 1 adult control or neuronal *xbp-1 s* (*rgef-1p::GFP or rab-3p::GFP*) animals carrying mutations for genes encoding neurotransmitter synthesis or signaling pathways stained with oil red O. All images are contrast matched and magnified between the pharynx and the most anterior part of the egg sac.

(B) Quantification of (A) using ImageJ as described in STAR Methods with control represented in gray and neuronal *xbp-1 s* represented in blue (light blue, *rgef-1p::xbp-1 s*; dark blue, *rab-3p::xbp-1 s*). Lines represent median and interquartile range, with each dot representing a single animal. ***p < 0.001 compared to *rab-3p::xbp-1 s* controls using Student's t test. *cat-2n*, *cat-2(n4547)*; *cat-2e*, *(cat-2e1112)*; *dop-1*, *dop-1(LX0645)*; *dop-1v*, *dop-1(vs101)*.

pan-neuronal *xbp-1s*, the beneficial effects of dopaminergic *xbp-1s* was completely dependent on *xbp-1* (Figure 4F; Figures S4A and S4B). These data indicate that dopaminergic *xbp-1s* signals a unique program distinct from serotonergic signaling, which acts through dopamine to mobilize lipids by increasing EHBP-1-mediated lipophagy. Indeed, knockdown of *ehbp-1* is sufficient to suppress the lipid depletion found in dopaminergic *xbp-1s* animals (Figures S4A and S4B). In agreement, the lipid depletion found in increased dopamine signaling through mutation of the dopamine reuptake receptor is also dependent on *xbp-1s* and *ehbp-1* (Figures S4C and S4D). Taken together, our data provide evidence that dopaminergic signaling promotes lipid depletion through XBP-1-mediated activation of EHBP-1, which is sufficient to extend lifespan and is independent of protein chaperone induction.

Serotonergic and Dopaminergic UPR^{ER} Signatures Are Unique and Independent

Next, we sought to determine whether serotonergic and dopaminergic UPR^{ER} were truly independent of each other. First, we performed transcriptome analysis on serotonergic *xbp-1s* and dopaminergic *xbp-1s* animals. As expected, these animals exhibit increased *xbp-1s*, as measured by qPCR, and overall UPR^{ER} signatures similar to pan-neuronal *xbp-1s* (Figures 5A and 5B). Moreover, consistent with our previous findings, serotonergic *xbp-1s* significantly increases mRNA transcript abundance of *hsp-4*, as well as another XBP-1 s target, *crt-1*, similar to pan-neuronal *xbp-1s*. Moreover, serotonergic *xbp-1s* broadly upregulates protein-folding genes and has a signature more similar to pan-neuronal *xbp-1s*, whereas dopaminergic *xbp-1s* either minimally affects or completely fails to promote expression of these genes (Figures 5A, 5C, and 5D). Finally, dopaminergic *xbp-1s* showed increased levels of the desaturase *fat-7,* similar to pan-neuronal *xbp-1s*, whereas serotonergic *xbp-1s* failed to upregulate these transcripts (Figure 5A).

In addition to transcriptional changes, we found that peripheral chaperone induction driven by serotonergic *xbp-1s* was independent of dopamine production, and mutations in *cat-2* had no effect on *hsp-4p::GFP* induction (Figures S5A and S5B). In addition, the lifespan extension and ER stress resistance found in serotonergic *xbp-1s* was completely independent of dopamine synthesis (Figures S5C and S5D). Similarly, the lipid depletion found in dopaminergic *xbp-1s* animals was completely independent of serotonin production, as mutations in *tph-1* did not suppress the lipid reduction found in these animals (Figures S6A and S6B). The lifespan extension found in dopaminergic *xbp-1s* animals was also completely independent of serotonin (Figure S6C). Finally, we found that the lifespan extension and ER stress resistance of dopaminergic and serotonergic *xbp-1s* are additive (Figures 6A and 6B), providing additional evidence that the two signaling modalities are truly distinct and unique.

DISCUSSION

Neuronal transmission of stress signals has been identified in multiple stress response pathways (Durieux et al., 2011; Prahlad et al., 2008; Taylor and Dillin, 2013). For the UPR^{ER}, recent work has identified that two distinct signaling modalities exist to affect whole-animal physiology and lifespan: first, chaperone induction drives protein homeostasis; and second, enhanced lipophagy by EHBP-1 drives lipid depletion. These systems were independent of each other and equally important for driving the beneficial effects of neuronal *xbp-1s* overexpression (Daniele et al., 2020). Here, we found that these paradigms diverge at the source of the neurons that drive the ER stress signal: serotonergic *xbp-1s* drives non-autonomous activation of chaperones to promote protein homeostasis and dopaminergic *xbp-1s* drives non-

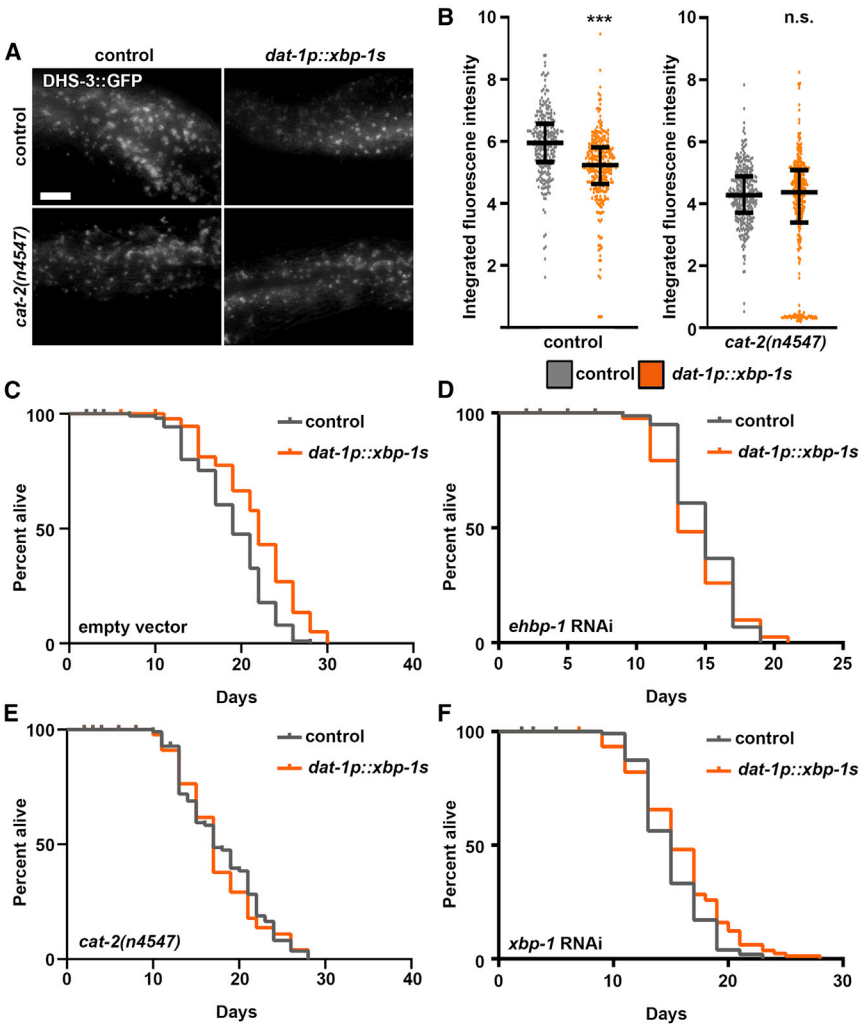

Figure 4. Overexpression of *xbp-1s* in Dopaminergic Neurons Drives Lipid Depletion to Extend Lifespan

(A) Representative fluorescent micrographs of intestinal lipid droplets (LDs) (by *dhs-3p::DHS-3::GFP*) in day 2 adult control and dopaminergic *xbp-1s* (*dat-1p::xbp-1s*) animals with and without *cat-2(n4547)* mutation in dopamine synthesis. Imaging was performed equidistant from the vulva to the tail of the worm across all conditions. All images are contrast matched. Scale bar represents 10 μm.

(B) Quantification of *dhs-3p::DHS-3::GFP* in (a) of control (gray) and dopaminergic *xbp-1s* (*dat-1p::xbp-1s;* orange) animals with and without *cat-2(n4547)* mutation in dopamine synthesis. Lines represent median and interquartile range, with each dot representing a single animal. Data are representative of three independent trials. ***p < 0.001 using non-parametric Mann-Whitney testing against matching control.

(C) Lifespans of control and dopaminergic *xbp-1s* (*dat-1p::xbp-1s*) animals grown on empty vector. Data are representative of three independent trials. See Table S1–S2 for lifespan statistics.

(D) Lifespans of control and dopaminergic *xbp-1s* (*dat-1p::xbp-1s*) animals grown on *ehbp-1* RNAi from hatch. Data are representative of three independent trials. See Table S1–S2 for lifespan statistics.

(E) Lifespan measurements of control and dopaminergic *xbp-1s* (*dat-1p::xbp-1s*) animals carrying *cat-2(n4547)* mutation for dopamine synthesis. Data are representative of three independent trials. See Table S1–S2 for lifespan statistics.

(F) Lifespans of control and dopaminergic *xbp-1s* (*dat-1p::xbp-1s*) animals grown on *xbp-1* RNAi. Data are representative of three independent trials. See Table S1–S2 for lifespan statistics. Measurements for (D), (E), and (F) were performed simultaneously and can be directly compared.

autonomous activation of lipophagy to promote lipid homeostasis. These two divergent signals are independently sufficient to drive beneficial effects on lifespan and together make up at least part of the neuronal circuitry involved in pan-neuronal *xbp-1s* signaling (Figure 6C). Interestingly, we found that the combination of serotonergic and dopaminergic *xbp-1s* caused an egg-laying defect, which was more severe than is found in pan-neuronal *xbp-1s* animals. Moreover, the transcriptional landscape of the combination was significantly different from the pan-neuronal *xbp*-1s animals. Thus, it is clear that the combination of the two individual signaling paradigms is not completely equivalent to pan-neuronal *xbp-1s*, despite that they show an additive phenotype for lifespan and resistance to ER stress. This may be due to differences in dosage or the requirement to mobilize other neuronal subtypes to fully phenocopy pan-neuronal *xbp-1s*.

Because we use RNAi in our experiments, it is possible that *xbp-1* RNAi is directly affecting our neuronal *xbp-1s* expression, despite neurons being refractory to RNAi. Therefore, more stringent tissue-specific studies are required for more conclusive evidence that *xbp-1s* is required directly in the periphery, but our data strongly suggest this is the case. Thus, it would be interesting to determine how two distinct signals can exist downstream of a single transcription factor, XBP-1s, solely based on which neuron elicits the non-autonomous stress signal. It is possible that based on which neuronal signal is received, peripheral tissues (e.g., the intestine), modify their response by recruiting variable cofactors for *xbp-1s* to drive a unique transcriptional program. Our work also invites the intriguing possibility of the existence of other neuronal populations involved (e.g., glutaminergic and GABAergic), which either work in concert with—or independent of—the serotonergic and dopaminergic circuits described. Indeed, our preliminary screens correlate glutamatergic and GABAergic neurons in chaperone induction and glutamatergic, GABAergic, and octopaminergic neurons in lipid metabolism. Although these neurons were not further investigated in this study due to their pleiotropic phenotypes, including severe motor defects, it is possible that these circuits play an additional role in signaling ER stress. More importantly, it is possible that one of these circuits—or some other neuronal circuit not studied

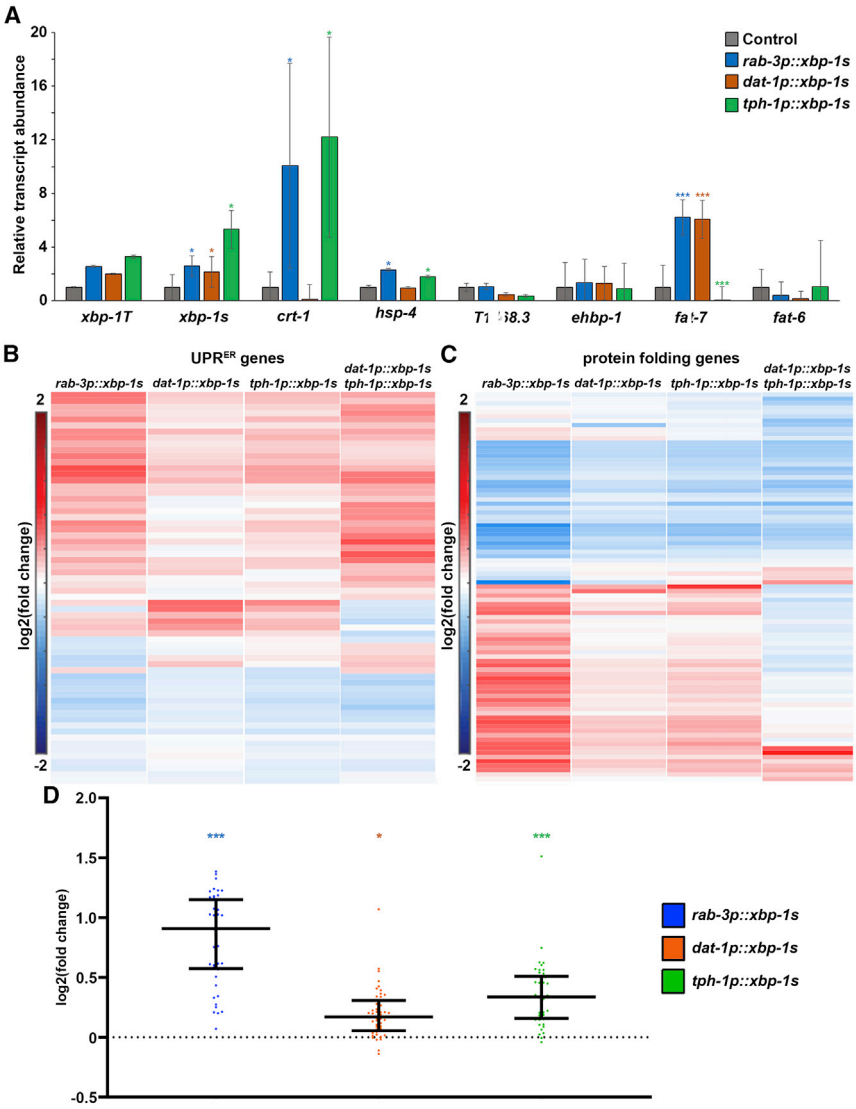

Figure 5. Serotonergic and Dopaminergic *xbp-1s* Elicit Two Different Transcriptional Programs

(A) qPCR of transcripts in control (gray), pan-neuronal *xbp-1s* (blue), dopaminergic *xbp-1s* (orange), and serotonergic *xbp-1s* (green) animals grown on empty vector from hatch. RNA was isolated in day 1 adults, and data were collected against a standard curve to calculate relative transcript abundance against control. Data are pooled across three biological replicates and four technical replicates per sample. Data are represented as mean ± standard deviation. *p < 0.05; ***p < 0.001 using Student's t test.

(B) RNA sequencing (RNA-seq) was performed in control, pan-neuronal *xbp-1s*, dopaminergic *xbp-1s*, serotonergic *xbp-1s*, and dopaminergic/serotonergic double *xbp-1s* as described in the STAR Methods. Heatmap indicates log2 (fold change) of genes in comparison to control. Here, canonical UPR^{ER} target genes are represented as genes that showed decreased expression when *ire-1* was mutated (Shen et al., 2005) and/or are part of the Gene Ontology (GO) term 0030968 UPR^{ER} using BioMart WormBase Parasite. Warmer colors indicate increased expression, and cooler colors indicate decreased expression. See Table S3 for actual values of log2 (fold change).

(C) Heatmap indicates log2 (fold change) of genes in comparison to control. Here, protein-folding genes are represented as per GO term 0006457 using BioMart WormBase Parasite. Warmer colors indicate increased expression, and cooler colors indicate decreased expression. See Table S4 for actual values of log2 (fold change).

(D) log2 (fold change) of genes are shown for all upregulated genes of pan-neuronal *xbp-1s* (blue), dopaminergic *xbp-1s* (orange), and serotonergic *xbp-1s* (green) of protein-folding genes represented as per GO term 0006457 using BioMart WormBase Parasite (bottom half of heatmap of C). Middle line represents median, and whiskers represent interquartile range. ***p < 0.001; *p < 0.05 using Mann-Whitney testing calculated from normalized reads of each gene compared to wild-type control.

here—feeds into the serotonergic circuit. We found that although serotonin is necessary for non-autonomous induction of protein homeostasis, it was not sufficient, as increasing serotonin signaling by mutation of the serotonin reuptake receptor had no effect on UPR^{ER}. Moreover, the suppression of chaperone induction in pan-neuronal *xbp-1s* by mutation of serotonin biosynthesis was not complete, suggesting an attractive hypothesis that some other neurotransmitter is responsible for the remainder of the signaling. Finally, serotonergic *xbp-1s* itself, although sufficient to induce chaperones, created a bimodal population. Taken together, these data clearly indicate the complexity of serotonin-mediated non-autonomous signaling, and further dissection of all neurons and their neurotransmitters is required to properly map the neuronal circuitry involved.

It is still unclear how serotonergic *xbp-1s* and dopaminergic *xbp-1s* signal two unique events. One possible reason is that increased *xbp-1s* in neurons non-specifically promotes the release of neurotransmitters, potentially by increasing release of SCVs, resulting in increased release of serotonin by serotonergic neurons and dopamine by dopaminergic neurons. Ultimately, it is the neurotransmitter itself that drives unique responses, for which dopamine promotes lipid depletion and serotonin—likely with other neurotransmitters—promotes protein homeostasis. Indeed, we found that increased dopamine signaling by mutations of the dopamine reuptake receptor decreased lipid levels in an *xbp-1*-dependent manner.

Another intriguing phenomenon from this study was the opposing role of serotonergic and dopaminergic signaling on lipid homeostasis. Although dopaminergic *xbp-1s* promoted lipid depletion, which had direct implications on organismal health, serotonergic *xbp-1s* resulted in increased levels of lipid droplets. One possible explanation is that downstream of serotonin

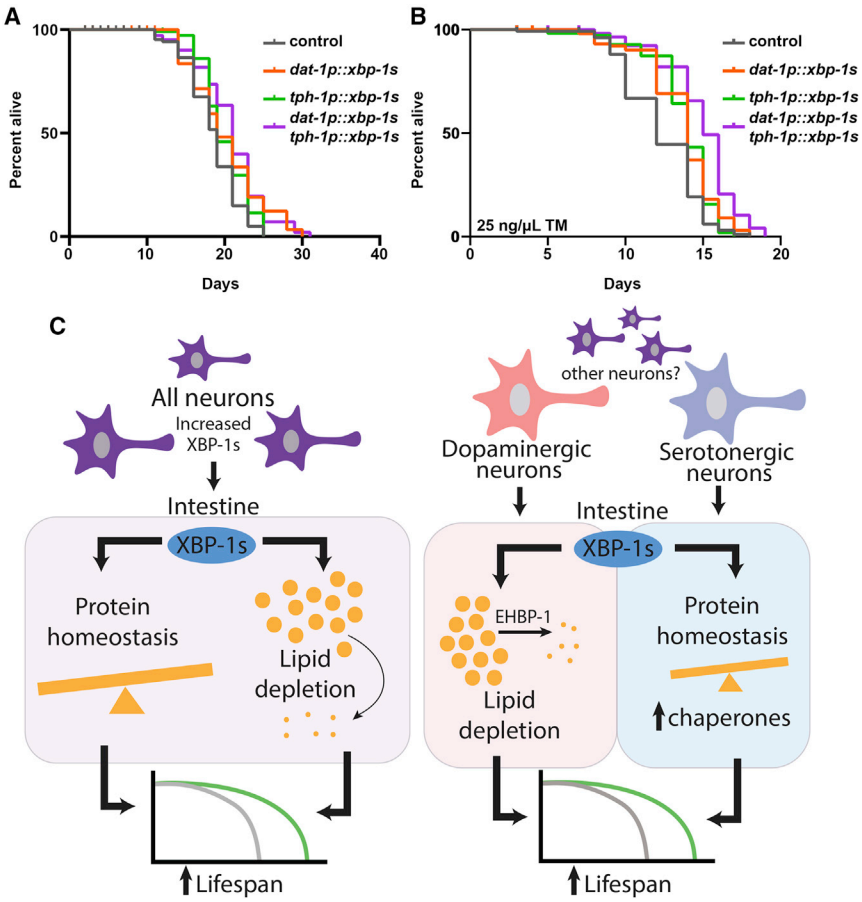

Figure 6. Serotonergic and Dopaminergic Neurons Have Independent Roles in Modulating Unique Branches of Non-autonomous UPR^{ER}

(A) Lifespan measurements of control, serotonergic *xbp-1s* (*tph-1p::xbp-1s*), dopaminergic *xbp-1 s* (*dat-1p::xbp-1s*), and serotonergic *xbp-1 s* (*tph-1p::xbp-1s*)/dopaminergic *xbp-1s* (*dat-1p::xbp-1s*) animals. Data are representative of three independent trials. See Table S1–S2 for lifespan statistics.

(B) TM survival assay of control, serotonergic *xbp-1s* (*tph-1p::xbp-1s*), dopaminergic *xbp-1s* (*dat-1p::xbp-1s*), and serotonergic *xbp-1s* (*tph-1p::xbp-1s*)/dopaminergic *xbp-1s* (*dat-1p::xbp-1s*) animals. Animals were moved to 25 ng/µL TM plates at day 1 of adulthood. Data are representative of three independent trials. See Table S1–S2 for lifespan statistics.

(C) Schematic/model showing pan-neuronal *xbp-1s* overexpression results in lifespan extension by two independent mechanisms: activation of chaperones to promote protein homeostasis and activation of an EHBP-1-mediated lipophagy machinery to deplete lipids. Serotonergic *xbp-1s* is sufficient to drive chaperone induction to ER stress resistance and extend lifespan but fails to activate EHBP-1-mediated lipophagy. In contrast, dopaminergic *xbp-1s* drives depletion of lipids through EHBP-1 but fails to activate chaperones to promote protein homeostasis. These divergent signals are independent and together impart the beneficial impact of pan-neuronal overexpression of *xbp-1s* on whole-animal physiology.

signaling, XBP-1 s is recruited primarily to the promoters of genes involved in protein homeostasis. This may titrate XBP-1 s away from genes involved in lipid homeostasis, which may result in a global increase in lipid levels. Indeed, we found that *fat-7* transcript levels, which increase in both pan-neuronal and dopaminergic *xbp-1s*, were decreased in serotonergic *xbp-1s*. Finally, it is interesting that although dopaminergic *xbp-1s* animals fail to induce chaperones, they exhibit increased resistance to tunicamycin, a drug that causes ER stress by blocking N-linked glycosylation and producing protein misfolding stress. Consistent with these findings, two recent studies showed that promoting lipid homeostasis by oleic acid supplementation or hyperactivation of lysosomal lipases was sufficient to drive protein homeostasis by promoting clearance of aggregation-prone proteins, despite not directly promoting chaperone induction (Imanikia et al., 2019a, 2019b). Thus, it is possible that promoting lipid homeostasis is sufficient to drive protein homeostasis in the absence of chaperones in the periphery. Still to be determined is whether this is due to a causative and direct impact of lipids on protein homeostasis or an indirect effect for which there is a decreased burden on ER, such that quality-control machinery can be mobilized strictly to regulate protein homeostasis.

Overall, the major finding that there exists two distinct and independent mechanisms of UPR^{ER} and that they are separable at the source of the neurons involved in signaling these effects is intriguing. Although this phenomenon is described in *C. elegans*, non-autonomous UPR^{ER} transmission is well-described in animal models, such as from the brain to the liver in mice (Brandt et al., 2018; Williams et al., 2014). Moreover, dopamine signaling has direct implications on lipid homeostasis and overall metabolism in higher eukaryotes (Folgueira et al., 2019; Fulton and Alquier, 2019; Leite and Ribeiro, 2020), which invites the attractive hypothesis that dopamine and serotonin signaling may play critical roles in diverging UPR^{ER} signals in higher eukaryotes.

STAR★METHODS

Detailed methods are provided in the online version of this paper and include the following:

- KEY RESOURCES TABLE
- RESOURCE AVAILABILITY
  - Lead Contact
  - Materials Availability
  - Data and Code Availability
- EXPERIMENTAL MODEL AND SUBJECT DETAILS
  - *C. elegans* strains and maintenance

- pVR1 (cloned into pre-existing pRT5 plasmid using PstI/XmaI restriction cloning, replacing rgef-1p for dat-1p)
- pRHS55 (cloned into pre-existing pRT5 plasmid using gibson assembly to replace rgef-1p with tph-1p)

- METHOD DETAILS
  - Stereomicroscopy for fluorescent transcriptional reporters
  - Lifespan and survival analysis
  - Oil Red O Staining
  - qPCR
  - RNA-sequencing
- QUANTIFICATION AND STATISTICAL ANALYSIS
  - Stereomicroscopy
  - Oil Red O
  - Large particle biosorter analysis
  - Lifespan and survival
  - qPCR
  - RNA-seq

SUPPLEMENTAL INFORMATION

Supplemental Information can be found online at https://doi.org/10.1016/j.celrep.2020.108489.

ACKNOWLEDGMENTS

We are grateful to all the members of the Dillin lab for intellectual and technical support, especially Melissa Sanchez and Anel Esquivel. This work was supported by grant 1K99AG065200-01A1 through the National Institute on Aging (NIA) to R.H.-S., the Bert Lubin Scholarship Fund through CHORI to M.d.l.R.R., and 4R01AG042679-04 through the NIA and the Howard Hughes Medical Institute to A.D. Some strains were provided by the CGC, which is funded by the NIH Office of Research Infrastructure Programs (P40 OD010440).

AUTHOR CONTRIBUTIONS

R.H.-S. and J.D. developed the story and performed or designed all strain construction, experiments, and data analysis. R.H.-S. wrote the manuscript and prepared figures, J.D. prepared artwork for figures. N.K., S.H., and S.M. performed lifespan and fluorescent imaging/quantification. M.d.l.R.R. performed RNA-seq analysis and assisted in quantification. G.G. constructed strains. S.D. performed fluorescent imaging experiments. J.R.D. and V.R. helped in conceptualization of the manuscript. A.S. assisted in data quantification. S.U.T. performed lifespans. L.J. performed essential experimental assistance. A.D. developed the story and assisted in experimental design and manuscript preparation.

DECLARATION OF INTERESTS

The authors declare no competing interests.

Received: July 29, 2020
Revised: October 20, 2020
Accepted: November 12, 2020
Published: December 8, 2020

REFERENCES

Barros, A.G.d.A., Bridi, J.C., de Souza, B.R., de Castro Júnior, C., de Lima Torres, K.C., Malard, L., Jorio, A., de Miranda, D.M., Ashrafi, K., and Romano-Silva, M.A. (2014). Dopamine signaling regulates fat content through β-oxidation in Caenorhabditis elegans. PLoS One *9*, e85874.

Bar-Ziv, R., Frakes, A.E., Higuchi-Sanabria, R., Bolas, T., Frankino, P.A., Gildea, H.K., Metcalf, M.G., and Dillin, A. (2020). Measurements of Physiological Stress Responses in C. Elegans. Journal of visualized experiments : JoVE. https://doi.org/10.3791/61001.

Berendzen, K.M., Durieux, J., Shao, L.-W., Tian, Y., Kim, H.-E., Wolff, S., Liu, Y., and Dillin, A. (2016). Neuroendocrine Coordination of Mitochondrial Stress Signaling and Proteostasis. Cell *166*, 1553–1563.e10.

Brandt, C., Nolte, H., Henschke, S., Engström Ruud, L., Awazawa, M., Morgan, D.A., Gabel, P., Sprenger, H.-G., Hess, M.E., Günther, S., et al. (2018). Food Perception Primes Hepatic ER Homeostasis via Melanocortin-Dependent Control of mTOR Activation. Cell *175*, 1321–1335.e20.

Chase, D.L., Pepper, J.S., and Koelle, M.R. (2004). Mechanism of extrasynaptic dopamine signaling in Caenorhabditis elegans. Nat. Neurosci. *7*, 1096–1103.

Daniele, J.R., Esping, D.J., Garcia, G., Parsons, L.S., Arriaga, E.A., and Dillin, A. (2017). "High-Throughput Characterization of Region-Specific Mitochondrial Function and Morphology". Sci. Rep. *7*, 6749.

Daniele, J.R., Higuchi-Sanabria, R., Durieux, J., Monshietehadi, S., Ramachandran, V., Tronnes, S.U., Kelet, N., Sanchez, M., Metcalf, M.G., Garcia, G., et al. (2020). UPRER promotes lipophagy independent of chaperones to extend life span. Sci. Adv. *6*, eaaz1441.

Durieux, J., Wolff, S., and Dillin, A. (2011). The cell-non-autonomous nature of electron transport chain-mediated longevity. Cell *144*, 79–91.

Escorcia, W., Ruter, D.L., Nhan, J., and Curran, S.P. (2018). Quantification of Lipid Abundance and Evaluation of Lipid Distribution in Caenorhabditis elegans by Nile Red and Oil Red O Staining. J. Vis. Exp., 57352.

Folgueira, C., Beiroa, D., Porteiro, B., Duquenne, M., Puighermanal, E., Fondevila, M.F., Barja-Fernández, S., Gallego, R., Hernández-Bautista, R., Castelao, C., et al. (2019). Hypothalamic dopamine signaling regulates brown fat thermogenesis. Nat. Metab. *1*, 811–829.

Frakes, A.E., and Dillin, A. (2017). The UPR^{ER}: Sensor and Coordinator of Organismal Homeostasis. Mol. Cell *66*, 761–771.

Frakes, A.E., Metcalf, M.G., Tronnes, S.U., Bar-Ziv, R., Durieux, J., Gildea, H.K., Kandahari, N., Monshietehadi, S., and Dillin, A. (2020). Four glial cells regulate ER stress resistance and longevity via neuropeptide signaling in *C. elegans*. Science *367*, 436–440.

Fulton, S., and Alquier, T. (2019). Lipid signalling in the mesolimbic dopamine pathway. Neuropsychopharmacology *44*, 221–222.

Heifetz, A., Keenan, R.W., and Elbein, A.D. (1979). Mechanism of action of tunicamycin on the UDP-GlcNAc:dolichyl-phosphate Glc-NAc-1-phosphate transferase. Biochemistry *18*, 2186–2192.

Higuchi-Sanabria, R., Charalel, J.K., Viana, M.P., Garcia, E.J., Sing, C.N., Koenigsberg, A., Swayne, T.C., Vevea, J.D., Boldogh, I.R., Rafelski, S.M., and Pon, L.A. (2016). Mitochondrial anchorage and fusion contribute to mitochondrial inheritance and quality control in the budding yeast Saccharomyces cerevisiae. Mol. Biol. Cell *27*, 776–787.

Imanikia, S., Sheng, M., Castro, C., Griffin, J.L., and Taylor, R.C. (2019a). XBP-1 Remodels Lipid Metabolism to Extend Longevity. Cell Rep. *28*, 581–589.e4.

Imanikia, S., Özbey, N.P., Krueger, C., Casanueva, M.O., and Taylor, R.C. (2019b). Neuronal XBP-1 Activates Intestinal Lysosomes to Improve Proteostasis in C. elegans. Curr. Biol. *29*, 2322–2338.e7.

Leite, F., and Ribeiro, L. (2020). Dopaminergic Pathways in Obesity-Associated Inflammation. J. Neuroimmune Pharmacol. *15*, 93–113.

Lints, R., and Emmons, S.W. (1999). Patterning of dopaminergic neurotransmitter identity among Caenorhabditis elegans ray sensory neurons by a TGFbeta family signaling pathway and a Hox gene. Development *126*, 5819–5831.

Na, H., Zhang, P., Chen, Y., Zhu, X., Liu, Y., Liu, Y., Xie, K., Xu, N., Yang, F., Yu, Y., et al. (2015). Identification of lipid droplet structure-like/resident proteins in Caenorhabditis elegans. Biochim. Biophys. Acta *1853*, 2481–2491.

Nagatsu, T., Levitt, M., and Udenfriend, S. (1964). Tyrosine hydroxylase. The initial step in norepinephrine biosynthesis. J. Biol. Chem. *239*, 2910–2917.

Prahlad, V., Cornelius, T., and Morimoto, R.I. (2008). Regulation of the cellular heat shock response in Caenorhabditis elegans by thermosensory neurons. Science *320*, 811–814.

Ranganathan, R., Sawin, E.R., Trent, C., and Horvitz, H.R. (2001). Mutations in the Caenorhabditis elegans serotonin reuptake transporter MOD-5 reveal serotonin-dependent and -independent activities of fluoxetine. J. Neurosci. *21*, 5871–5884.

Salio, C., Lossi, L., Ferrini, F., and Merighi, A. (2006). Neuropeptides as synaptic transmitters. Cell Tissue Res. *326*, 583–598.

Serrano-Saiz, E., Poole, R.J., Felton, T., Zhang, F., De La Cruz, E.D., and Hobert, O. (2013). Modular control of glutamatergic neuronal identity in C. elegans by distinct homeodomain proteins. Cell *155*, 659–673.

Shen, X., Ellis, R.E., Sakaki, K., and Kaufman, R.J. (2005). Genetic interactions due to constitutive and inducible gene regulation mediated by the unfolded protein response in C. elegans. PLoS genetics *1*, e37.

Sze, J.Y., Victor, M., Loer, C., Shi, Y., and Ruvkun, G. (2000). Food and metabolic signalling defects in a Caenorhabditis elegans serotonin-synthesis mutant. Nature *403*, 560–564.

Tatum, M.C., Ooi, F.K., Chikka, M.R., Chauve, L., Martinez-Velazquez, L.A., Steinbusch, H.W.M., Morimoto, R.I., and Prahlad, V. (2015). Neuronal serotonin release triggers the heat shock response in C. elegans in the absence of temperature increase. Curr. Biol. *25*, 163–174.

Taylor, R.C., and Dillin, A. (2013). XBP-1 is a cell-nonautonomous regulator of stress resistance and longevity. Cell *153*, 1435–1447.

Westmoreland, J.J., McEwen, J., Moore, B.A., Jin, Y., and Condie, B.G. (2001). Conserved function of Caenorhabditis elegans UNC-30 and mouse Pitx2 in controlling GABAergic neuron differentiation. J. Neurosci. *21*, 6810–6819.

Williams, K.W., Liu, T., Kong, X., Fukuda, M., Deng, Y., Berglund, E.D., Deng, Z., Gao, Y., Liu, T., Sohn, J.-W., et al. (2014). Xbp1s in Pomc neurons connects ER stress with energy balance and glucose homeostasis. Cell Metab. *20*, 471–482.

Xue, D., Finney, M., Ruvkun, G., and Chalfie, M. (1992). Regulation of the mec-3 gene by the C.elegans homeoproteins UNC-86 and MEC-3. EMBO J. *11*, 4969–4979.

Zhang, P., Na, H., Liu, Z., Zhang, S., Xue, P., Chen, Y., Pu, J., Peng, G., Huang, X., Yang, F., et al. (2012). Proteomic study and marker protein identification of Caenorhabditis elegans lipid droplets. Mol. Cell. Proteomics *11*, 317–328.

STAR★METHODS

KEY RESOURCES TABLE

REAGENT or RESOURCE	SOURCE	IDENTIFIER
Bacterial and Virus Strains		
OP50	CGC	N/A
HT115	CGC	N/A
DH5α	Invitrogen	N/A
Chemicals, Peptides, and Recombinant Proteins		
(+)-5-Fluorodeoxyuridine (FUDR)	Spectrum Chemical	F2026-10GMBL
Agarose, low melting	Sigma-Aldrich	A9414-10G
Alexa Fluor 488 Phalloidin	Life Technologies	A12380
Bacto Peptone	Fisher Scientific	DF0118072
BD Difco granulated agar	VWR	90000-782
Calcium chloride dihydrate	VWR	97061-904
Carbenicillin	BioPioneer	C0051-25
Chloroform	Sigma-Aldrich	34854
Cholesterol	Sigma-Aldrich	57-88-5
IPTG dioxane free	Denville Scientific	CI8280-4
Isopropanol	Fisher Scientific	AC327272500
LB Broth Miller	Fisher Scientific	BP1426500
Magnesium sulfate heptahydrate	VWR	EM-MX0070-3
Potassium phosphate dibasic	VWR	EM-PX1570-2
Potassium phosphate monobasic	VWR	EM-PX1565-5
Sodium Chloride	EMD Millipore	SX0420-5
Sodium phosphate dibasic	VWR	71003-472
Tetracycline hydrochloride	Sigma-Aldrich	T7660-5G
Trizol	Fisher Scientific	15596018
Tunicamycin	Millipore	654380
Critical Commercial Assays		
QIAquick PCR Purification Kit	QIAGEN	28106
QIAprep Spin Miniprep Kit	QIAGEN	27106
Deposited Data		
RNA-seq	Annotare 2.0 ArrayExpress	E-MTAB-9771
Experimental Models: Organisms/Strains		
C. elegans: Bristol (N2) strain as wild type (WT)	CGC	N2
C. elegans: AGD927: uthIs270 [rab-3p::Xbp-1 s, myo-2p::tdTomato]	Taylor and Dillin, 2013	N/A
C. elegans: AGD928: uthIs270[rab-3p::Xbp-1 s, myo-2p::tdTomato]; zcIs4[hsp-4p::GFP]	Taylor and Dillin, 2013	N/A
C. elegans: AGD1237: N2, unc-30(ok613) IV; uthIs270[rab-3p::Xbp-1 s, myo-2p::tdTomato]; zcIs4[hsp-4p::GFP]	This study	N/A
C. elegans: AGD1497: N2, uthIs270[rab-3p::Xbp-1 s, myo-2p::tdTomato]; zcIs4[hsp-4p::GFP];tbh1(n3247)	This study	N/A
C. elegans: AGD1498: N2, uthIs270[rab-3p::Xbp-1 s, myo-2p::tdTomato]; zcIs4[hsp-4p::GFP]; ttx-3(ks5)	This study	N/A

(*Continued on next page*)

Continued

REAGENT or RESOURCE	SOURCE	IDENTIFIER
C. elegans: AGD1500: N2, uthIs270[rab-3p::Xbp-1 s, myo-2p::tdTomato]; zcIs4[hsp-4p::GFP]; tph1(mg280)	This study	N/A
C. elegans: AGD1526: N2, uthIs270[rab-3p::Xbp-1 s, myo-2p::tdTomato]; zcIs4[hsp-4p::GFP] V; cat2(e1112)	This study	N/A
C. elegans: AGD1767: N2, uthIs460[dat-1p::Xbp-1 s, myo-2p::tdTomato]	This study	N/A
C. elegans: AGD1771: N2, uthIs464[rgef-1p::Xbp-1 s, myo-2p::tdTomato]	This study	N/A
C. elegans: AGD2048: dhs-3p::dhs-3::GFP; hjSi158 [vha-6p::SEL-1(1-79)::mCherry::HDELlet-858 3′ UTR]	Daniele et al., 2020	N/A
C. elegans: AGD2049: dat-1(ok157), dhs-3p::dhs-3::GFP; hjSi158[vha-6p::SEL-1(1-79)::mCherry::HDELlet-858 3′ UTR]	This study	N/A
C. elegans: AGD2064: N2, uthIs460[dat-1p::Xbp-1 s, myo-2p::tdTomato](#Aa), dhs-3p::dhs-3::GFP; hjSi158[vha-6p::SEL-1(1-79)::mCherry::HDELlet-858 3′ UTR]	This study	N/A
C. elegans: AGD2065: N2, dhs-3p::dhs-3::GFP; hjSi158 [vha-6p::SEL-1(1-79)::mCherry::HDELlet-858 3′ UTR]; uthIs270 [rab-3p::Xbp-1 s, myo-2p::tdTomato]	Daniele et al., 2020	N/A
C. elegans: AGD2149: N2, uthIs270[rab-3p::Xbp-1 s, myo-2p::tdTomato]; zcIs4[hsp-4p::GFP]; dop1(vs101)	This study	N/A
C. elegans: AGD2207: N2, cat-2(n4547) II; zcIs4 [hsp-4p::GFP]V	This study	N/A
C. elegans: AGD2209: N2, cat-2(n4547) II; dhs-3p::dhs-3::GFP; hjSi158[vha-6p::SEL-1(1-79)::mCherry::HDELlet-858 3′ UTR]	This study	N/A
C. elegans: AGD2147: N2, uthIs270[rab-3p::Xbp-1 s, myo-2p::tdTomato]; zcIs4[hsp-4p::GFP]; mec-3(e1338)IV	This study	N/A
C. elegans: AGD2155: N2, uthIs270[rab-3p::Xbp-1 s, myo-2p::tdTomato]; zcIs4[hsp-4p::GFP]; unc-43(n498)IV	This study	N/A
C. elegans: AGD2164: N2, uthIs460[dat-1p::xbp-1 s, myo-2p::tdTomato](#Aa); cat-2(n4547)	This study	N/A
C. elegans: AGD2275: N2, uthIs460[dat-1p::Xbp-1 s, myo-2p::tdTomato](#Aa); zcIs4(hsp-4p::GFP)V	This study	N/A
C. elegans: AGD2474: N2, uthIs460[dat-1p::xbp-1 s, myo-2p::tdTomato](#Aa); ldrIs [dhs-3p::dhs-3::GFP + unc-76(+)]; hjSi158[vha-6p::SEL-1(1-79)::mCherry::HDEL::let-858 3′ UTR]; cat-2(n4547) II	This study	N/A
C. elegans: AGD2496: N2, tph-1(mg280)II; ; zcIs4[hsp-4p::GFP]V	This study	This study
C. elegans: AGD2503: N2, uthIs501(tph-1p::xbp-1 s::unc-54 UTR; myo-2p::GFP) line1	This study	This study
C. elegans: AGD2504: N2, uthIs502(tph-1p::xbp-1 s::unc-54 UTR; myo-2p::GFP) line2	This study	This study

(*Continued on next page*)

Continued

REAGENT or RESOURCE	SOURCE	IDENTIFIER
C. elegans: AGD2505: N2, uthIs503(tph-1p::xbp-1 s::unc-54 UTR; myo-2p::GFP) line3	This study	This study
C. elegans: AGD2506: N2, uthIs501(tph-1p::xbp-1 s::unc-54 UTR; myo-2p::GFP) line1; zcls4[hsp-4p::GFP]V	This study	This study
C. elegans: AGD2507: N2, uthIs502(tph-1p::xbp-1 s::unc-54 UTR; myo-2p::GFP) line2; zcls4[hsp-4p::GFP]V	This study	This study
C. elegans: AGD2508: N2, uthIs503(tph-1p::xbp-1 s::unc-54 UTR; myo-2p::GFP) line3; zcls4[hsp-4p::GFP]V	This study	This study
C. elegans: AGD2686: N2, uthIs460[dat-1p::xbp-1 s, myo-2p::tdTomato], ldrIs[dhs-3p::dhs-3::GFP + unc-76(+)]; hjSi158[vha-6p::SEL-1(1-79)::mCherry::HDEL::let-858 3′ UTR]; tph-1(mg280)II	This study	This study
C. elegans: AGD2695: N2, uthIs460[dat-1p::xbp-1 s, myo-2p::tdTomato]; tph-1(mg280) II	This study	This study
C. elegans: AGD2713: N2, uthIs503(tph-1p::xbp-1 s::unc-54 UTR; myo-2p::GFP) line3; uthIs460[dat-1p::xbp-1 s, myo-2p::tdTomato]	This study	This study
C. elegans: AGD2714: N2, uthIs503(tph-1p::xbp-1 s::unc-54 UTR; myo-2p::GFP) line 3; ldrIs[dhs-3p::dhs-3::GFP + unc-76(+)]; hjSi158 [vha-6p::SEL-1(1-79)::mCherry::HDEL::let-858 3′ UTR]"	This study	This study
C. elegans: AGD2715: N2, uthIs503(tph-1p::xbp-1 s::unc-54 UTR; myo-2p::GFP) line3; cat-2(n4547)	This study	This study
C. elegans: AGD2716: N2, uthIs503(tph-1p::xbp-1 s::unc-54 UTR; myo-2p::GFP) 57E4; tph-1(mg280)	This study	This study
C. elegans: AGD2967: N2, *mod-5(n3314)*I, zcls4[hsp-4p::GFP]V	This study	This study
C. elegans: AGD2968: N2, *mod-5(n3314)*I, ldrIs [dhs-3p::dhs-3::GFP + unc-76(+)]; hjSi158[vha-6p::SEL-1(1-79)::mCherry::HDEL::let-858 3′ UTR]	This study	This study
C. elegans: MT15620: *tph-1(mg280)*	CGC	GR1321
C. elegans: MT15620: *cat-2(n4547)*	CGC	MT15620
C. elegans: RM2702: *dat-1(ok157)*	CGC	RM2702
C. elegans: SJ4005: zcls4(hsp-4p::GFP)V	Taylor and Dillin, 2013	SJ4005
Oligonucleotides		
RHS427 xbp-1T qPCR F	cacctccatcaacaacaacat	Forward primer to qPCR xbp-1 total
RHS428 xbp-1T qPCR R	aaccgtctgctccttcctcaa	Reverse primer to qPCR xbp-1 total
RHS429 xbp-1 s qPCR F	cgtgcctttgaatcagcagtg	Forward primer to qPCR xbp-1 spliced
RHS430 xbp-1 s qPCR R	cgaggtgtccatcttcttgtt	Reverse primer to qPCR xbp-1 spliced
RHS433 crt-1 qPCR F	atgacgagatggacggagaat	Forward primer to qPCR crt-1
RHS434 crt-1 qPCR R	ctgacttgacctgccacaaat	Reverse primer to qPCR crt-1
RHS435 T14G8.3 qPCF F	gccagtggagccaaaagcaaa	Forward primer to qPCR T14G8.3
RHS436 T14G8.3 qPCR R	ccaagcggttcatagcctctt	Reverse primer to qPCR T14G8.3
RHS473 hsp4 qPCR V2 F	GAATCAACCCTGACGAAGCAG	Forward primer to qPCR hsp-4

(*Continued on next page*)

Continued

REAGENT or RESOURCE	SOURCE	IDENTIFIER
RHS474 hsp4 qPCR V2 R	CCTCCGACAGTCTCAATACCC	Reverse primer to qPCR hsp-4
RHS475 ehbp-1 qPCR F	GATCCGTGAAACAGAAGTTGG	forward primer to qPCR ehbp-1
RHS476 ehbp-1 qPCR R	CCCAATTGGTCAATTTCCGAA	reverse primer to qpCR ehbp-1
RHS682 fat-6 qPCR F	TCTACCAGCTCATCTTCGAGGC	forward primer to qPCR fat-6
RHS683 fat-6 qPCR R	GATCACGAGCCCATTCGATGAC	reverse primer to qPCR fat-6
RHS684 fat-7 qPCR F	GGAAGGAGACAGCATTCATTGCG	forward primer to qPCR fat-7
RHS685 fat-7 qPCR R	GTCTTGTGGGAATGTGTGGTGG	reverse primer to qPCR fat-7
RHS529 tph1p-xbp1s F	AGGTCGACTCTAGAGGATCC cgcgaattgcggccgacata	forward primer to PCR tph-1p
RHS530 tph1p-xbp1s R	CGTTTTGGATAGTTGCTCAT atgattgaagagagcaatgctac	reverse primer to PCR tph-1p
RHS531 tph1p-xbp1s F2	gcattgctctcttcaatcatATGAGCAACTATC CAAAACGTATTTA	Forward primer to PCR xbp-1 s::UTR + vector from pAF18 (*3*)
RHS532 tph1p-xbp1s R2	tatgtcggccgcaattcgcgGGATCCTCTAG AGTCGACCTG	reverse primer to PCR xbp-1 s::UTR + vector from pAF18
VR1	CTGCAGaatgtttctagtcgtttttg	Forward primer to PCR dat-1p from gDNA
VR2	tttttatgggttttggtaggCCCGGG	Reverse primer to PCR dat-1p from gDNA
VR3	CCCGGGATGAGCAACTATCCAAAACG	Forward primer to PCR xbp-1 s::UTR + vector from pAF18 (*3*)
VR4	TGCAGGCATGCAAGCTTCTGCAG	Reverse primer to PCR xbp-1 s::UTR + vector from pAF18
Recombinant DNA		
pRHS55: tph-1p::xbp-1 s cDNA::unc-54 3′ UTR	This study	N/A
pVR1: dat-1p::xbp-1 s cDNA::unc-54 3′ UTR	This study	N/A
pRT5: pAD1 rgef-1p::xbp-1 s cDNA::unc-54 3′ UTR	Taylor and Dillin, 2013	N/A
pEK1: myo-2p::GFP::unc-54 3′UTR	This study	N/A
pEK2myo-2p::tdtomato::unc-52 3′ UTR	This study	N/A
Software and Algorithms		
Zen 2 Blue Edition	Zeiss	N/A – download available from Zeiss website
LASX	Leica	N/A – download available from Leica website

RESOURCE AVAILABILITY

Lead Contact

Please contact Andrew Dillin (dillin@berkely.edu), corresponding author, for any requests.

Materials Availability

All strains are available either at the Caenorhabditis Genome Center (CGC) or by request to the lead contact.

Data and Code Availability

All data is available in the main text or the supplementary materials. Raw sequencing data is available through ArrayExpress Annotaire 2.0, accession number: E-MTAB-9771. All other data can be requested from the lead contact.

EXPERIMENTAL MODEL AND SUBJECT DETAILS

C. elegans strains and maintenance

All *C. elegans* strains are derivatives of the Bristol N2 strain from Caenorhabditis Genetics Center (CGC) and are listed in Key Resources Table. For standard maintenance of worms, animals are grown on standard nematode growth media (NGM) plates and fed OP50 *E. coli* B bacteria at 15°C, for a maximum of 25 generations. For all experiments, animals are synchronized using a standard bleaching protocol where carcasses are degraded using a bleach solution (1.8% sodium hypochlorite, 0.375M KOH), followed by 3

washed with M9 solution (22 mM KH_2PO_4 monobasic, 42.3 mM Na_2HPO_4, 85.6 mM NaCl, 1 mM $MgSO_4$), followed by L1 arresting synchronization, which is performed by floating eggs in M9 overnight in a 20°C incubator on a rotator for a maximum of 16 hours. L1 arresting was performed to better age-match animals, as some mutants and transgenic animals used in this study exhibit some variability in growth rates. All experiments were performed without L1-arresting at least once to ensure that there were no artifacts produced from L1-arresting. Synchronized animals were plated on RNAi bacteria (NGM + 1 μM IPTG and 100 μg/mL carbenicillin; HT115 *E. coli* K strain containing pL4440 vector control or pL4440 with RNAi of interest) until the desired stage of adulthood. All RNAi constructs used in this study were isolated from the Vidal library or previously characterized (Daniele et al., 2020).

Transgene integration was performed by injecting N2 worms with pVR1 (*dat-1p::xbp-1 s*) or pRHS55 (*tph-1p::xbp-1 s*) at 25 ng/μL, pEK2 (*myo-2p::tdtomato*) for pVR1 or pEK1 (*myo-2p::GFP*) for pRHS55 at 2.5 ng/μL and 100 ng/μL of pD64 vehicle as filler DNA. Worms positive for fluorescent pharynx were selected to identify for stable arrays. Integration was performed by gamma irradiation. Briefly, L4 worms were irradiated with 4000-4400 rems of radiation and integrants were identified by selecting animals that maintained fluorescent pharynxes at 100% frequency in the F3 generation. Multiple independent lines were isolated, backcrossed to N2 animals 8x to eliminate mutations, and animals with the most similar phenotypes to the array animals were used for further experimentation.

pVR1 (cloned into pre-existing pRT5 plasmid using PstI/XmaI restriction cloning, replacing rgef-1p for dat-1p)

dat-1p

aatgtttctagtcgtttttgtattttaaagcacattcccaattctgaatacttttctgaaatccatgaaatggaacttgaatccagttttcactaaaacgacctcatacactttctctcgtatcct
caaaatatctatgacattatcattagcttcgctagtttcatttctttcaaatattatgcattcttaaattccgatacccgcgtgcaaaagtgctctattgagcaactttgggatcatatgtaca
caccaatgccctttcccaaatcttttcctgtccttttctctaaaaacaataaatccatgcctattccagtatgacccctttgaagcagatataatcgcacaaacatatacacatagctcg
gataaatgtagaaaaagaagaaaagaagtataagtagatagatgctttccggcaattatccaccgcaccgtagtcttcaccaactgagactgcgtcgttaggagacgccgacatg
attcagaagcagaatttggaagaaaaacgacgatgatattgaggctggcacacatacaccggaatattcgacatgccaccacatctagattccaaggcaatctctacctcttccca
ttctttcggttttttgttctgacaagaaaagtggatagctacgggctcaatgagctgattttatttttaaatatcttaaaactatactagattcatgtgttttcaggtccatattccaaattagtc
gaaaagctgatcccgctacggtttactcgaatctcaacaatttttagcc

xbp-1 s

ATGAGCAACTATCCAAAACGTATTTATGTGCTCCCAGCACGCCACGTGGCAGCGCCACAGCCTCAGAGAATGGCTCCCAAGCGTG
CACTTCCAACAGAACAAGTTGTCGCACAACTTCTTGGCGATGATATGGGACCATCTGGGCCACGCAAAAGAGAACGACTGAATCAT
TTGAGTCAGGAGGAGAAAATGGATCGTCGGAAACTTAAAAATCGAGTCGCAGCCCAAAATGCTAGAGACAAAAAGAAGGAAAGATC
AGCAAAGATCGAGGATGTGATGCGCGATCTGGTGGAGGAGAACCGCCGGCTCCGCGCTGAAAACGAACGTCTTCGCCGTCAAA
ATAAAAATCTTATGAACCAGCAGAACGAGTCCGTCATGTATATGGAAGAGAACAACGAAAACTTGATGAACAGCAATGATGCATGCA
TCTACCAGAACGTCGTCTACGAAGAAGAAGTCGTCGGTGAGGTTGCACCAGTTGTCGTCGTCGGAGGAGAGGATCGCCGTGCCTT
TGAATCAGCAGTGGGAACAGGCCCGATCCACCTCCATCAACAACAACATCAGCAACCAACTCCGTCGTATGGATTCCAAGAAGAA
CAACACAATCAGTGTGGATATGTATCTAACTATCATCTCGATTCTATGCAACCACATGGATCGCAACAAGAAGATGGACACCTCGAA
CAAATCCTCGAACATCTCAAGAGCCCAAGCGGAGAGTTCGATCGATTCGTTGCTGGCTACATTGAGGAAGGAGCAGACGGTTATGC
AGCGTCTTGTTCAAGCGGATCCATGTACACATCTTCAGAAACGCGTGAAACACTTTCGCCGAATTCCCTAGCCATGTCCCCGTCGA
TGAGCAGCTCGAGCACTGACTGGGATGATGAGCTTTTGGGATGTGGAACCGAAACTGGAACTGGAACCGACGAGCTGCTTACCGA
CCCCGGAAACTGGAACTTTGAAACTTTCGACGAAAATTCAATCGACCTAAATTTCTTCCAAAATTAA

unc-54 3′ UTR

CATCTCGCGCCCGTGCCTCTGACTTCTAAGTCCAATTACTCTTCAACATCCCTACATGCTCTTTCTCCCTGTGCTCCCACCCCCTA
TTTTTGTTATTATCAAAAAACTTCTCTTAATTTCTTTGTTTTTTAGCTTCTTTTAAGTCACCTCTAACAATGAAATTGTGTAGATTCAAAAA
TAGAATTAATTCGTAATAAAAAGTCGAAAAAAATTGTGCTCCCTCCCCCCATTAATAATAATTCTATCCCAAAATCTACACAATGTTC
TGTGTACACTTCTTATGTTTTTTACTTCTGATAAATTTTTTTGAAACATCATAGAAAAAACCGCACACAAAATACCTTATCATATGTTAC
GTTTCAGTTTATGACCGCAATTTTTATTTCTTCGCACGTCTGGGCCTCTCATGACGTCAAATCATGCTCATCGTGAAAAAGTTTTGGA
GTATTTTTGGAATTTTTCAATCAAGTGAAAGTTTATGAAATTAATTTTCCTGCTTTTGCTTTTTGGGGTTTCCCCTATTGTTTGTCAAGA
TTTCGAGGACGGCGTTTTTCTTGCTAAAATCACAAGTATTGATGAGCACGATGCAAGAAAGATCGGAAGAAGGTTTGGGTTTGAGG
CTCAGTGGAAG

pRHS55 (cloned into pre-existing pRT5 plasmid using gibson assembly to replace rgef-1p with tph-1p)

tph-1p

cgcgaattgcggccgacatattgaaagaatgaaatataaattacgtttttgaataaaaaattttaaaatggtaactagaatataaacgttcaaatttagaacacgtattaaacataaatt
tgattgaaaaatttttgaaatcaaattcaatttcttcgaaaaacttgaataaccaaaaaaaaagtttttgaaaacatttgttcaaatattgtagatattgtagaaattggttttcacacagctttt
gggtattcagttttcgtgttccaacaagaaaataatgaaatcttcaagagatgaaatttggatttttacaaaaacacggtctgtaacttggctgaaaatgaaaataattaataaaattgat
aaaatattgcaaaatatttcacagttactattcaacattattttgctattaaaattcaaaagatgttgatttatgactagtacatcagaacagttttcaaaaatttttgatggtttttgggagaatg
ccttttactctgtgtaactcaaaaaataattggcaattgtttgtaataaaaagtatttcaaaagaaagaaaaattgtttcttatgattttatcagttgatcattcgttttctagacatgtatttttct
agatatgctagtttgaatctacacaatttagtgagtttgaatttagattccagcgatatgcaatgattttgaagttaatgagtatttgcctgtttttactaggtcattccaaaaatttcaactgc
agaactcaacactgaaccttaaggtaaagcgaaatctgaacttttttttgctagtttgagttttttattttaagagatcgaaaaattttccttgaactttgaaacatgacaattcaaacttttca
aatgtagtaagctccgatgcgttcccgttcattattcttcttcaataaattcgaaatctgacatcattctcatcttttcccatcatcacaagccgtgggctcatttattctcccacggaaacc
atgacagcaaaaataaatagagtggcgccttattcgactcatttcgttttttttctccggatattagattgtgtggcaggcggctccattgtatattacgtgccgaattccagaagcacca

cgccatcggatatctaaaagaggaggtgtctttgtttgcgcataataaaacaatcaatcaacacagcaaagacccctctcaacctcatttcatgattttctttggtttttaggtagcattgc
tctcttcaatcat

xbp-1 s

ATGAGCAACTATCCAAAACGTATTTATGTGCTCCCAGCACGCCACGTGGCAGCGCCACAGCCTCAGAGAATGGCTCCCAAGCGTG
CACTTCCAACAGAACAAGTTGTCGCACAACTTCTTGGCGATGATATGGGACCATCTGGGCCACGCAAAAGAGAACGACTGAATCA
TTTGAGTCAGGAGGAGAAAATGGATCGTCGGAAACTTAAAAATCGAGTCGCAGCCCAAAATGCTAGAGACAAAAAGAAGGAAAGAT
CAGCAAAGATCGAGGATGTGATGCGCGATCTGGTGGAGGAGAACCGCCGGCTCCGCGCTGAAAACGAACGTCTTCGCCGTCAAA
ATAAAAATCTTATGAACCAGCAGAACGAGTCCGTCATGTATATGGAAGAGAACAACGAAAACTTGATGAACAGCAATGATGCATGCA
TCTACCAGAACGTCGTCTACGAAGAAGAAGTCGTCGGTGAGGTTGCACCAGTTGTCGTCGTCGGAGGAGAGGATCGCCGTGCCT
TTGAATCAGCAGTGGGAACAGGCCCGATCCACCTCCATCAACAACAACATCAGCAACCAACTCCGTCGTATGGATTCCAAGAAGA
ACAACACAATCAGTGTGGATATGTATCTAACTATCATCTCGATTCTATGCAACCACATGGATCGCAACAAGAAGATGGACACCTCGA
ACAAATCCTCGAACATCTCAAGAGCCCAAGCGGAGAGTTCGATCGATTCGTTGCTGGCTACATTGAGGAAGGAGCAGACGGTTAT
GCAGCGTCTTGTTCAAGCGGATCCATGTACACATCTTCAGAAACGCGTGAAACACTTTCGCCGAATTCCCTAGCCATGTCCCCGTC
GATGAGCAGCTCGAGCACTGACTGGGATGATGAGCTTTTGGGATGTGGAACCGAAACTGGAACTGGAACCGACGAGCTGCTTACC
GACCCCGGAAACTGGAACTTTGAAACTTTCGACGAAAATTCAATCGACCTAAATTTCTTCCAAAATTAA

unc-54 3′ UTR

CATCTCGCGCCCGTGCCTCTGACTTCTAAGTCCAATTACTCTTCAACATCCCTACATGCTCTTTCTCCCTGTGCTCCCACCCCCTAT
TTTTGTTATTATCAAAAAACTTCTCTTAATTTCTTTGTTTTTTAGCTTCTTTTAAGTCACCTCTAACAATGAAATTGTGTAGATTCAAAAAT
AGAATTAATTCGTAATAAAAAGTCGAAAAAAATTGTGCTCCCTCCCCCCATTAATAATAATTCTATCCCAAAATCTACACAATGTTCTG
TGTACACTTCTTATGTTTTTTACTTCTGATAAATTTTTTTGAAACATCATAGAAAAAACCGCACACAAAATACCTTATCATATGTTACGT
TTCAGTTTATGACCGCAATTTTTATTTCTTCGCACGTCTGGGCCTCTCATGACGTCAAATCATGCTCATCGTGAAAAAGTTTTGGAGT
ATTTTTGGAATTTTTCAATCAAGTGAAAGTTTATGAAATTAATTTTCCTGCTTTTGCTTTTTGGGGTTTCCCCTATTGTTTGTCAAGATTT
CGAGGACGGCGTTTTTCTTGCTAAAATCACAAGTATTGATGAGCACGATGCAAGAAAGATCGGAAGAAGGTTTGGGTTTGAGGCTCA
GTGGAAG

METHOD DETAILS

Stereomicroscopy for fluorescent transcriptional reporters

Fluorescent animals were grown on standard RNAi plates as described above until day 1 of adulthood. Animals were moved onto standard NGM plates containing 5 μL of 100 mM sodium azide to paralyze worms. Paralyzed worms were lined up and imaged immediately on a Leica M250FA automated fluorescent stereomicroscope equipped with a Leica DFC3000G camera, standard GFP filter, and driven by LAS-X software.

Lifespan and survival analysis

Lifespan measurements were performed on solid NGM plates with RNAi bacteria. Worms were synchronized as described above, and adult animals were moved away from their progeny daily onto fresh RNAi plates until no progeny were visible (~7-10 days). Animals were then scored every 1-2 days for death until all animals are scored. Animals with bagging, vulval explosion, or other age-unrelated deaths were censored and removed from quantification. For tunicamycin survival assays, animals are moved to plates containing 25 ng/μL tunicamycin at day 1 of adulthood. Animals are not proved for the duration of the experiment, as no progeny survive at this concentration of tunicamycin, and drug efficacy was not visibly reduced during the duration of the experiment. Animals are scored daily for tunicamycin survival for better dynamic range.

Oil Red O Staining

Staining of lipids using Oil Red O was performed as previously described (*18*). Briefly, day 1 adult animals were washed off plates with PBST (0.02% Tween 20) and washed three times in PBST to remove bacteria. Animals were fixed in 40% isopropanol for 3 minutes at room temperature, with proper mixing on a rotator. Animals were then stained with Oil Red O at a final concentration of 1% w/v in 60% isopropanol (Oil Red O solution was prepared by dissolving Oil Red O at 2% w/v in 100% isopropanol, then diluting into water to 60% and allowing this solution to mix by rocking on a nutator for 2 hours at room temperature, then filtering Oil Red O through a 0.2 μm cellulose sterile syringe filter. 600 μL was added to a 100 μL suspension of worms for a final concentration of 1% w/v). Staining was performed for 2 hours on a rotator at 20°C, then animals were washed by removing Oil Red O solution up to 100 μL, then adding in 600 μL of PBST and rotating for another 30 minutes at 20°C. Animals were then imaged on a Leica M250FA automated fluorescent stereomicroscope equipped with a Leica DFC310 FX color camera and driven by LAS-X software.

qPCR

Worms were grown on standard NGM plates with empty vector bacteria on solid agar from hatch at 20°C until D1. Worms were collected by washing off with M9. M9 was subsequently aspirated, replaced with trizol, and worms were freeze/thawed 3x with liquid nitrogen. After the final thaw, chloroform was added at a 1:5 ratio with chloroform:trizol volume for aqueous separation of RNA, which was performed via centrifugation in heavy gel phase-lock tubes. The aqueous phase was transferred into isopropanol, then RNA

purification was performed using a QIAGEN RNeasy Mini Kit (74106) as per manufacturer's directions. 2 μg of RNA was used for cDNA synthesis using the QIAGEN QuantiTect Reverse Transcriptase kit (205314) as per manufacturer's directions. qPCR analysis was performed using a general standard curve protocol using SYBR-green. Four technical replicates were performed for three independent biological replicates per sample. All primers are listed in Key Resources Table.

RNA-sequencing

Animals were synchronized and grown to D1 on EV RNAi plates. ~2,000 animals were harvested using M9. M9 was subsequently aspirated, replaced with trizol, and worms were freeze/thawed 3x with liquid nitrogen. After the final thaw, chloroform was added at a 1:5 ratio of chloroform:trizol for aqueous separation of RNA using heavy gel phase-lock tubes (VWR, 10847-802). The aqueous phase was mixed with isopropanol and RNA purification was performed using a QIAGEN RNeasy Mini Kit (74106) as per manufacturer's directions. Library preparation, RNA-sequencing, and analysis was performed by Genewiz. Briefly, library preparation was performed with Poly A selection and HiSeq Sequencing using NEBNext Ultra RNA Library Prep Kit for Illumina following manufacturer's instructions (NEB, Ipswich, MA, USA). Sequencing libraries were clustered onto 1 lane of a flowcell, loaded on Illumina HiSeq instrument (4000 or equivalent) and samples were sequenced using 2x150bp Paired End configuration. Base calling was conducted on HiSeq Control Software. Raw reads were trimmed to remove adapters and nucleotides with poor quality using Trimmomatic v.0.36, then mapped to the reference genome on ENSEMBL using STAR aligner v.1.5.2, counting genes that fell within exon regions. DESeq2 was used for differential expression analysis across groups of samples (three biological replicates per sample). p values were generated using the Wald test and adjusted using the Benjamini-Hochberg procedure.

QUANTIFICATION AND STATISTICAL ANALYSIS

All statistical information is presented in every figure legend, including sample size, number of replicates, and statistical analysis used. Detailed protocols for quantification and analysis are also provided below.

Stereomicroscopy

Quantification of screening data of *hsp-4p::GFP* animals were performed on ImageJ. Integrated fluorescent intensity measurements were made along the bottom portion of the animal starting at the lower spermathecal to the tail. Data is represented as integrated intensity normalized to the area of the region of interest drawn.

Oil Red O

Quantification was performed on ImageJ. Images were first stacked to RGB (Image = > Color = > Stack to RGB), then converted to a 32 bit black and white image (Image = > Type = > 32 bit). Images were then inverted, so that Oil Red O staining was recognized as the brightest points. Integrated density was measured across the anterior and posterior portions of the worm, ignoring the region where eggs were present. Anterior and posterior sections were first normalized to the area of the region of interest (ROI), then averaged to calculate integrated Oil Red O values.

Large particle biosorter analysis

For large-scale quantification of fluorescent animals, a Union Biometrica complex object parameter analysis sorter (COPAS) was used (Bar-Ziv et al., 2020). Fluorescent animals were washed off plates using M9, and run through the COPAS biosort using a 488 nm light source. Integrated fluorescent intensity was normalized to the time of flight of the animal, then normalized to the extinction to correct for both worm length and worm thickness. For experiments including transgenic animals with *myo-2p::GFP* co-injection markers, signal is only collected in the bottom 60% of animals to remove signal from the head. All biosorter data is represented dot-line plot, where the middle line represents median and the two outer lines represent interquartile range (the 25^{th} and 75^{th} percentile), and each dot represents a single animal. All experiments are performed at least three independent times, and statistics are calculated using Prism7 software and non-parametric Mann-Whitney testing.

Lifespan and survival

All survival data is represented as a Kaplan-Meier curve, and statistics are calculated using Log-Rank testing using Prism7 software. All experiments are performed at least three times, with all experiments performed by at least two independent researchers, with all conditions blinded each time

qPCR

Standard Student's t test was used for qPCR data.

RNA-seq

A proprietary pipeline was used by Genewiz to calculate p values provided in Tables S3 and S4. p values were generated using the Wald test and adjusted using the Benjamini-Hochberg procedure.